

Prediction of dual quantum spin Hall insulator in NbIrTe₄ monolayer

Xiangyang Liu,^{1,2} Junwen Lai,^{1,2} Jie Zhan,^{1,2} Tianye Yu,² Wujun Shi,^{3,4} Peitao Liu,^{1,2} Xing-Qiu Chen,^{1,2,*} and Yan Sun^{1,2,†}

¹*School of Materials Science and Engineering, University of Science and Technology of China, Shenyang 110016, China.*

²*Shenyang National Laboratory for Materials Science, Institute of Metal Research, Chinese Academy of Sciences, Shenyang 110016, China.*

³*Center for Transformative Science, ShanghaiTech University, Shanghai 201210, China*

⁴*Shanghai High Repetition Rate XFEL and Extreme Light Facility (SHINE), ShanghaiTech University, Shanghai 201210, China*

Dual quantum spin Hall insulator (QSHI) is a newly discovered topological state in the 2D material TaIrTe₄, exhibiting both a traditional Z_2 band gap at charge neutrality point and a van Hove singularity (VHS) induced correlated Z_2 band gap with weak doping. Inspired by the recent progress in theoretical understanding and experimental measurements, we predicted a promising dual QSHI in the counterpart material of the NbIrTe₄ monolayer by first-principles calculations. In addition to the well-known band inversion at the charge neutrality point, two new band inversions were found after CDW phase transition when the chemical potential is near the VHS, one direct and one indirect Z_2 band gap. The VHS-induced non-trivial band gap is around 10 meV, much larger than that from TaIrTe₄. Furthermore, since the new generated band gap is mainly dominated by the 4d orbitals of Nb, electronic correlation effects should be relatively stronger in NbIrTe₄ as compared to TaIrTe₄. Therefore, the dual QSHI state in the NbIrTe₄ monolayer is expected to be a good platform for investigating the interplay between topology and correlation effects.

I. INTRODUCTION AND MOTIVATION

Two-dimensional (2D) materials with VHS near the Fermi level are ideal platforms for studying the interplay between topological electronic structure and correlation effects[1–11]. As a typical layered material, TaIrTe₄ monolayer was predicted to be a 2D topological insulator with a band gap around 32 meV[12–14]. Very recently, a new quantum topological state of dual QSHI was discovered in the TaIrTe₄ monolayer by the observation of quantized longitudinal conductance, which is rare in other QSHIs[15]. It was found that, in addition to the QSHI state at the charge neutrality point, two new non-trivial Z_2 gaps are generated when the Fermi level shifts to the VHS points by weak electron and hole doping effects, respectively.

Owing to the divergence of density of states (DOSs), a CDW phase transition is induced when the Fermi level shifts to the VHSs, resulting in the correlated Z_2 band gap. Different from traditional Z_2 band gaps, the VHSs generated topological band gap is expected to naturally relate to the novel correlated electronic topological states of the fractional quantum spin Hall effect and helical quantum spin liquid[16–22]. Though the VHSs generated Z_2 band gap and integer quantized longitudinal conductance can exist in TaIrTe₄, the corresponding fractional topology and other strongly correlated topological states have, so far, not been observed. Therefore, it is necessary to find out some more materials candidates that host both topology and correlation[23–31]. One possible

reason for the absence of strongly correlated topological phenomena in TaIrTe₄ is the weak strength of electron correlation. With this inspiration, we analyzed the dual Z_2 topological state in NbIrTe₄, an isoelectronic counterpart of TaIrTe₄. Due to the difference between Ta-5d and Nb-4d orbitals near VHSs, the electronic correlation effect is expected to be more pronounced in NbIrTe₄ than in TaIrTe₄. This makes the NbIrTe₄ to be a good candidate material for observing the correlated topological phenomena that are absent in TaIrTe₄.

II. RESULT AND DISCUSSION

The crystal structure of a NbIrTe₄ monolayer shares the same structural prototype as 1T'-MoTe₂ monolayer[32] and features a sandwich-like structure, as depicted in Fig. 1(a). In this arrangement, the Nb and Ir atoms are positioned in the middle layer, forming parallel zigzag chains along the b -axis. Each Nb or Ir atom is surrounded by six Te atoms, forming a distorted octahedron. Fig. 1(c) shows the energy dispersion along the high-symmetry lines (Fig. 1(b)) calculated by employing Vienna Ab initio Simulation Package (VASP)[33] with generalized gradient approximation (GGA) of the Perdew-Burke-Ernzerhof (PBE) approximation[34]. One can observe that a band inversion exists near the X point with a band gap of around 35 meV, in agreement with previous reports[13, 35]. In addition, two VHSs are located around Γ and X , respectively, with the former one above the Fermi level and the latter below the Fermi level. Correspondingly, two narrow peaks of DOSs generated from the VHSs can be found above and below the Fermi level with energy of $\sim E_F + 60$ meV and $\sim E_F - 60$ meV, respectively. From the orbital projected band structure

* xingqiu.chen@imr.ac.cn

† sunyan@imr.ac.cn

and DOS, the two VHSs below and above the Fermi level are dominated by the $4d$ orbitals of Nb and hence a strong correlation is expected here. With the above understanding of the electronic band structure near the Fermi level, we projected the Bloch wavefunctions into maximally localized Wannier functions (MLWFs) and constructed effective tight binding model Hamiltonians based on the overlaps of these Wannier orbitals[36].

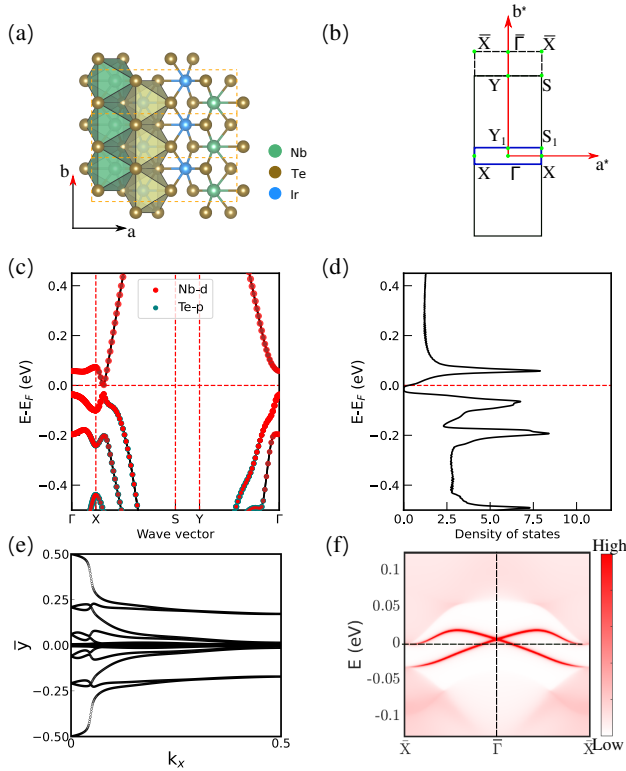


FIG. 1. Crystal and electronic structure of NbIrTe₄ monolayer. (a) Top view of the crystal structure. (b) Two-dimensional (2D) Brillouin zone (BZ) and its projection along the c -axis for both the primitive cell and CDW supercell. The high-symmetry lines are denoted as follows: Γ -X-S-Y for the primitive cell, Γ -X-S₁-Y₁ for the $1 \times 20 \times 1$ supercell, and Γ - \bar{X} for the edge lines along the b -axis. (c) Energy dispersion along high-symmetry lines of NbIrTe₄ monolayer primitive cell. (d) Density of states of NbIrTe₄ monolayer primitive cell. (e) Wannier charge center evolution with Fermi level fixed at charge neutrality point. (f) Energy dispersion of edge state of NbIrTe₄ monolayer primitive cell.

To verify the topological state, we calculated the Wannier center evolution and edge state with chemical potential locating at the charge neutrality point[37]. The Wannier center evolution in Fig. 1(e) presents as a zigzag form with changing partner at the edges of $k_x=0$ and π/a , which is a typical feature in Z_2 topological insulators[38]. Consistent with the bulk state analysis, the edge state with open boundary condition along the b -axis direction shows linear band crossing at the Γ point and connects the occupied and unoccupied bulk bands. Hence, the Z_2

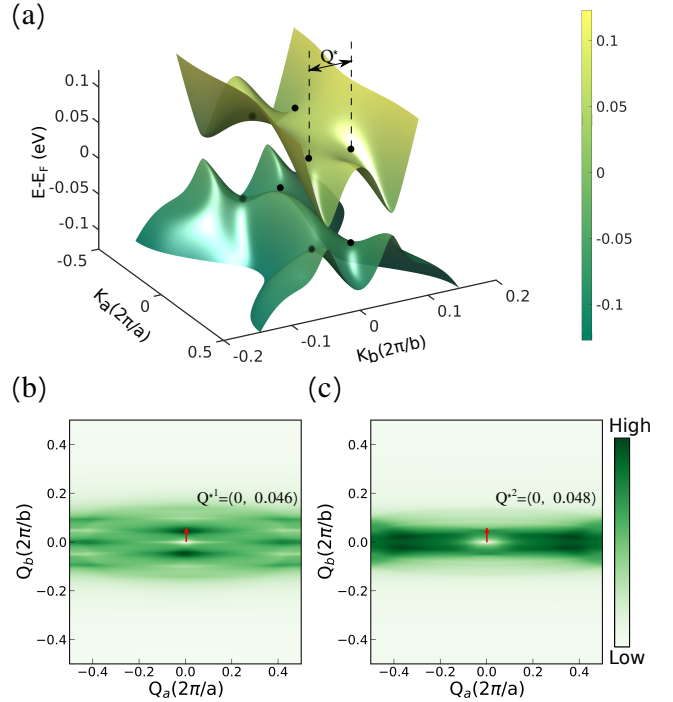


FIG. 2. Band structure and charge susceptibility in NbIrTe₄ monolayer primitive cell. (a) Three dimensional (3D) plot of energy dispersion ($k_a - k_b - E$) and location of van Hove singularities near the Fermi level. (b, c) Charge susceptibility of NbIrTe₄ with chemical potential at VHSs level of the valence and conduction bands, respectively.

band gap at the charge neutrality point can be confirmed from both bulk band order and edge Dirac point.

In order to identify the detailed positions of the VHSs near the charge neutrality point, we plot the energy dispersion of band- $n_{occ} + 2$ and band- $n_{occ} - 2$ in the whole 2D Brillouin zone (BZ), where n_{occ} refers to the index of the highest occupied band in a primitive cell considering the spin. As presented in Fig. 2(a), the four VHS points on band- $n_{occ} + 2$ are located at $(0.211 \frac{2\pi}{a}, 0.024 \frac{2\pi}{b})$, and its inversion and mirror partners. Considering the one-dimensional Nb-chains are similar to the Ta-chains in TaIrTe₄, the wavevectors along the b direction roughly corresponds to $1 \times 20 \times 1$ and $1 \times 21 \times 1$ supercells for the nearby VHSs on band- $n_{occ} + 2$ and band- $n_{occ} - 2$, respectively.

We further calculated the charge susceptibility by shifting the chemical potential at $\sim E_F + 60$ meV and $\sim E_F - 60$ meV, corresponding to the position of VHSs on band- $n_{occ} + 2$ and band- $n_{occ} - 2$, respectively. The charge susceptibility $\chi(\mathbf{q})$ at a given energy is computed by following the formula of the Lindhard function $\chi(\mathbf{q}) = \sum \frac{f_{\mathbf{k}}(1-f_{\mathbf{k}+\mathbf{q}})}{\varepsilon_{\mathbf{k}+\mathbf{q}} - \varepsilon_{\mathbf{k}} + i\delta}$, where f refers to the Fermi-Dirac distribution, ε is a momentum-dependent energy and δ refers to the broadening in data processing. Guided by the fact

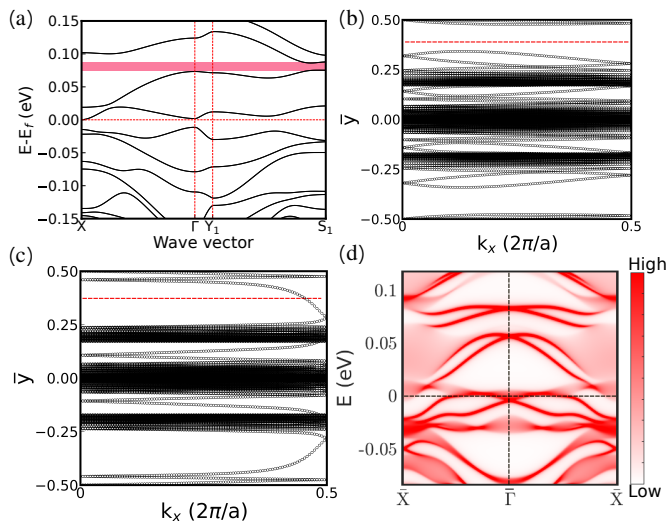


FIG. 3. Band structure and topological properties in CDW phase. (a) Energy dispersion along high symmetry lines. The pink range represent the VHS generated Z_2 band gap. (b-c) Wannier charge center evolutions with Fermi level lying at E_0 and $E_0 + 80$ meV, respectively. (d) Energy dispersion of edge states.

that the direction of \mathbf{Q} is parallel to the Ta-chains in the TaIrTe₄ monolayer[15], we specifically chose a vector aligned with the Nb-chains in the NbIrTe₄ monolayer prior to further analysis. From Fig. 2(b) and (c), one can see that a local maximum of the charge susceptibility is located at the wavevectors of $\mathbf{Q}^{*1} = (0, 0.046 \frac{2\pi}{a})$ and $\mathbf{Q}^{*2} = (0, 0.048 \frac{2\pi}{b})$ for the valence bands and conduction bands, respectively. Therefore, a CDW phase transition may occur when the chemical potential is shifted to near $\sim E_F + 60$ meV and $\sim E_F - 60$ meV via weak doping or gating effects.

The wavevectors of $\mathbf{Q}^{*1} = (0, 0.046 \frac{2\pi}{a})$ and $\mathbf{Q}^{*2} = (0, 0.048 \frac{2\pi}{b})$ in Fig. 2 can be described by the supercell of $1 \times 21 \times 1$ and $1 \times 20 \times 1$, respectively. To study the possible CDW phase transition, we constructed an effective Hamiltonian model for a supercell of $1 \times 20 \times 1$ based on the overlaps of Wannier orbitals. Following the Fröhlich-Peierls Hamiltonian approach with supercell along the b -axis and only the intra-orbital interaction considered, the CDW modulated electronic band structure can be described by $H = H_r + V \cos(Qy) \psi_r^\dagger \psi_r$ [39]. Here, V represents the potential induced by the superlattice. The periodicity of this potential is determined by the parameter Q , which can be identified by examining \mathbf{Q}^* in Fig. 2.

By increasing the potential V , a new band gap emerges near $E_F + 80$ meV, originating from the original VHSs, as illustrated by the pink range in Fig. 3(a). However, when the potential V was varied from 0.01 eV to 0.15 eV, no indirect band gap was observed between band- N_{occ} and band- $N_{occ} - 10$ for the VHSs below the charge neutrality point. Here N_{occ} refers to the index of the

highest occupied band in a supercell, taking into account the spin. This lack of an indirect band gap may be attributed to the competition between the detailed shape of the electronic band structure and the strength of the modulation potential. From Fig. 3(a), one can see that there are two global band gaps in the energy window from $\sim E_F - 150$ meV to $\sim E_F + 150$ meV. One is located at the charge neutrality point and the other one is generated between the band- $N_{occ} + 4$ and band- $N_{occ} + 6$. The band gaps at and above the charge neutrality point are around 15 and 10 meV, respectively, when the modulation potential V is set to 0.1 eV.

To check the topological charge of these two gaps, we calculated the bulk Wannier center evolutions and energy dispersions of edge states. Fig. 3(b) shows the Wannier center evolutions by modulating the chemical potential at the charge neutrality point. One can observe that each pair of evolution lines exhibits a fixed partner and becomes degenerate at two time-reversal-invariant points $k_x = 0$ and π/a . Therefore, the Wannier center evolutions do not intersect with the reference lines, indicating that the gap at the charge neutrality point is topologically trivial. However, the Wannier center evolutions switch partners at $k_x = 0$ and π/a while keeping the occupied bands fixed at band- $N_{occ} + 4$, as depicted in Fig. 3(c). The zigzag pattern of the Wannier center evolutions ensures an odd number of intersections with the reference lines, resulting in a non-trivial Z_2 band gap.

The topological phases were further checked by calculating edge states with open boundary conditions along the b -axis. From the energy dispersion illustrated in Fig. 3(d), we are mainly interested in the three zones that are indexed by the energy windows of $\sim E_F - 0.04$ eV to $\sim E_F + 0.01$ eV, $\sim E_F + 0.01$ eV to $\sim E_F + 0.06$ eV, and $\sim E_F + 0.06$ eV to $\sim E_F + 0.1$ eV. In the first region, although edge bands are present within the bulk band gap, they intersect the Fermi level twice. Consequently, these edge states lack topological protection and can be eliminated through external perturbations, consistent with the behavior exhibited by the Wannier center evolutions depicted in Fig. 3(b). In the second region, we observe a Dirac-point-like edge band structure connecting the bulk states originating from band- $N_{occ} + 2$ and band- $N_{occ} + 4$, as depicted in Fig. 3(a). Notably, there exists a noticeable band anti-crossing between band- $N_{occ} + 2$ and band- $N_{occ} + 4$ around the X point, although there is no indirect band gap present. Therefore, the band structure resulted from band- $N_{occ} + 2$ and band- $N_{occ} + 4$ forms a non-trivial Z_2 topological semimetal state when considering the CDW modulation potential. This differs from the case in monolayer TaIrTe₄, where a direct non-trivial Z_2 band gap of approximately 5 meV is formed by band- $N_{occ} + 2$ and band- $N_{occ} + 4$.

While there is not a global band gap between band- $N_{occ} + 2$ and band- $N_{occ} + 4$, we do observe a direct gap formed by band- $N_{occ} + 4$ and band- $N_{occ} + 6$ in the range of $\sim E_F + 60$ meV to $\sim E_F + 100$ meV. From the edge energy dispersion in this energy window, one can observe

that a Dirac-point state connecting the bulk bands originating from original band- $N_{occ} + 4$ and band- $N_{occ} + 6$. It is a typical feature of a 2D Z_2 topological insulator and fully agreement with the analysis from Wannier charge evolutions in Fig. 3(c). Therefore, NbIrTe₄ is expected to undergo a CDW phase transition along the b -axis direction and results in two non-trivial Z_2 band gap. One is a direct band gap with a globally semimetallic nature, and the other one is an indirect band gap of around 10 meV. Since both gaps are not far away from the charge neutrality point, they can be achieved via weak electron doping or gating.

III. CONCLUSION

In summary, we have predicted a dual QSHI state in monolayer NbIrTe₄ via first-principles calculations. In addition to the original non-trivial Z_2 band gap at the charge neutrality point, a new global Z_2 band gap of around 10 meV can be obtained when the chemical potential is shifted to the VHS point in the electron doping

range. Besides, an indirect band inversion in the CDW phase was found in the energy window around $E_0 + 20$ meV to $E_0 + 30$ meV near the X point. Since both of these two nontrivial band gaps are close to the charge neutrality point, they are expected to be experimentally detected after weak electron doping or gating. Moreover, the VHS point above the Fermi level is mainly dominated by the $4d$ orbitals of Nb. In comparison with Ta- $5d$ orbitals in TaIrTe₄, the dual QSHI state in NbIrTe₄ should manifest a strong correlation effect and some more correlated topological states are expected.

ACKNOWLEDGMENTS

This work was supported by the National Key R&D Program of China (Grant No. 2021YFB3501503), the National Natural Science Foundation of China (Grants No. 52271016 and No. 52188101), and Foundation from Liaoning Province (Grant No. XLYC2203080). Part of the numerical calculations in this study were carried out on the ORISE Supercomputer.

-
- [1] L. Wang, E.-M. Shih, A. Ghiotto, L. Xian, D. A. Rhodes, C. Tan, M. Claassen, D. M. Kennes, Y. Bai, B. Kim, *et al.*, “Correlated electronic phases in twisted bilayer transition metal dichalcogenides,” *Nature materials*, vol. 19, no. 8, pp. 861–866, 2020.
- [2] G.-B. Liu, D. Xiao, Y. Yao, X. Xu, and W. Yao, “Electronic structures and theoretical modeling of two-dimensional group-vib transition metal dichalcogenides,” *Chemical Society Reviews*, vol. 44, no. 9, pp. 2643–2663, 2015.
- [3] Y.-T. Hsu, A. Vaezi, M. H. Fischer, and E.-A. Kim, “Topological superconductivity in monolayer transition metal dichalcogenides,” *Nature communications*, vol. 8, no. 1, pp. 1–6, 2017.
- [4] L. Wei, Q. Xu, Y. He, Q. Li, Y. Huang, W. Zhu, K. Watanabe, T. Taniguchi, M. Claassen, D. A. Rhodes, D. M. Kennes, L. Xian, A. Rubio, and L. Wang, “Linear resistivity at van Hove singularities in twisted bilayer WSe₂,” *Proceedings of the National Academy of Sciences*, vol. 121, p. e2321665121, Apr. 2024.
- [5] K. Kim, S. Kim, J. S. Kim, H. Kim, J.-H. Park, and B. I. Min, “Importance of the van Hove singularity in superconducting PdTe₂,” *Phys. Rev. B*, vol. 97, p. 165102, Apr. 2018.
- [6] S. Xu, M. M. Al Ezzi, N. Balakrishnan, A. Garcia-Ruiz, B. Tsim, C. Mullan, J. Barrier, N. Xin, B. A. Piot, T. Taniguchi, K. Watanabe, A. Carvalho, A. Mishchenko, A. K. Geim, V. I. Fal’ko, S. Adam, A. H. C. Neto, K. S. Novoselov, and Y. Shi, “Tunable van Hove singularities and correlated states in twisted monolayer-bilayer graphene,” *Nature Physics*, vol. 17, pp. 619–626, May 2021.
- [7] S. Wu, Z. Zhang, K. Watanabe, T. Taniguchi, and E. Y. Andrei, “Chern insulators, van Hove singularities and topological flat bands in magic-angle twisted bilayer graphene,” *Nature Materials*, vol. 20, pp. 488–494, Apr. 2021.
- [8] K. Lee, G. F. Lange, L.-L. Wang, B. Kuthanazhi, T. V. Trevisan, N. H. Jo, B. Schruck, P. P. Orth, R.-J. Slager, P. C. Canfield, and A. Kaminski, “Discovery of a weak topological insulating state and van Hove singularity in triclinic RhBi₂,” *Nature Communications*, vol. 12, p. 1855, Mar. 2021.
- [9] M. Kang, L. Ye, S. Fang, J.-S. You, A. Levitan, M. Han, J. I. Facio, C. Jozwiak, A. Bostwick, E. Rotenberg, M. K. Chan, R. D. McDonald, D. Graf, K. Kaznatcheev, E. Vescovo, D. C. Bell, E. Kaxiras, J. van den Brink, M. Richter, M. Prasad Ghimire, J. G. Checkelsky, and R. Comin, “Dirac fermions and flat bands in the ideal kagome metal FeSn,” *Nature Materials*, vol. 19, pp. 163–169, Feb. 2020.
- [10] Y. Xu, B. Yan, H.-J. Zhang, J. Wang, G. Xu, P. Tang, W. Duan, and S.-C. Zhang, “Large-gap quantum spin hall insulators in tin films,” *Phys. Rev. Lett.*, vol. 111, p. 136804, Sept. 2013.
- [11] B. Sun, W. Zhao, T. Palomaki, Z. Fei, E. Runburg, P. Malinowski, X. Huang, J. Cenker, Y.-T. Cui, J.-H. Chu, X. Xu, S. S. Ataei, D. Varsano, M. Palummo, E. Molinari, M. Rontani, and D. H. Cobden, “Evidence for equilibrium exciton condensation in monolayer WTe₂,” *Nature Physics*, vol. 18, pp. 94–99, Jan. 2022.
- [12] P.-J. Guo, X.-Q. Lu, W. Ji, K. Liu, and Z.-Y. Lu, “Quantum spin hall effect in monolayer and bilayer TaIrTe₄,” *Physical Review B*, vol. 102, no. 4, p. 041109, 2020.
- [13] J. Liu, H. Wang, C. Fang, L. Fu, and X. Qian, “Van der waals stacking-induced topological phase transition in layered ternary transition metal chalcogenides,” *Nano letters*, vol. 17, no. 1, pp. 467–475, 2017.
- [14] A. Marrazzo, M. Gibertini, D. Campi, N. Mounet, and N. Marzari, “Relative abundance of Z_2 topological order

- in exfoliable two-dimensional insulators,” *Nano letters*, vol. 19, no. 12, pp. 8431–8440, 2019.
- [15] J. Tang, T. S. Ding, H. Chen, A. Gao, T. Qian, Z. Huang, Z. Sun, X. Han, A. Strasser, J. Li, *et al.*, “Dual quantum spin hall insulator by density-tuned correlations in TaIrTe₄,” *Nature*, vol. 628, no. 8008, pp. 515–521, 2024.
- [16] J. Maciejko, X.-L. Qi, A. Karch, and S.-C. Zhang, “Fractional topological insulators in three dimensions,” *Physical review letters*, vol. 105, no. 24, p. 246809, 2010.
- [17] L. Santos, T. Neupert, S. Ryu, C. Chamon, and C. Mudry, “Time-reversal symmetric hierarchy of fractional incompressible liquids,” *Physical Review B*, vol. 84, no. 16, p. 165138, 2011.
- [18] M. Goerbig, “From fractional chern insulators to a fractional quantum spin hall effect,” *The European Physical Journal B*, vol. 85, pp. 1–8, 2012.
- [19] W. Li, D. Sheng, C. Ting, and Y. Chen, “Fractional quantum spin hall effect in flat-band checkerboard lattice model,” *Physical Review B*, vol. 90, no. 8, p. 081102, 2014.
- [20] C. Wang and T. Senthil, “Time-reversal symmetric $u(1)$ quantum spin liquids,” *Physical Review X*, vol. 6, no. 1, p. 011034, 2016.
- [21] M. Barkeshli, P. Bonderson, M. Cheng, and Z. Wang, “Symmetry fractionalization, defects, and gauging of topological phases,” *Physical Review B*, vol. 100, no. 11, p. 115147, 2019.
- [22] K.-S. Park and H. Han, “Dirac quantization and fractional magnetoelectric effect in interacting topological insulators,” *Physical Review B*, vol. 82, no. 15, p. 153101, 2010.
- [23] N. J. Ghimire and I. I. Mazin, “Topology and correlations on the kagome lattice,” *Nature materials*, vol. 19, no. 2, pp. 137–138, 2020.
- [24] S. Paschen and Q. Si, “Quantum phases driven by strong correlations,” *Nature Reviews Physics*, vol. 3, no. 1, pp. 9–26, 2021.
- [25] M. Z. Hasan and C. L. Kane, “Colloquium: Topological insulators,” *Rev. Mod. Phys.*, vol. 82, pp. 3045–3067, Nov. 2010.
- [26] X. Teng, L. Chen, F. Ye, E. Rosenberg, Z. Liu, J.-X. Yin, Y.-X. Jiang, J. S. Oh, M. Z. Hasan, K. J. Neubauer, B. Gao, Y. Xie, M. Hashimoto, D. Lu, C. Jozwiak, A. Bostwick, E. Rotenberg, R. J. Birgeneau, J.-H. Chu, M. Yi, and P. Dai, “Discovery of charge density wave in a kagome lattice antiferromagnet,” *Nature*, vol. 609, pp. 490–495, Sept. 2022.
- [27] J.-X. Yin, B. Lian, and M. Z. Hasan, “Topological kagome magnets and superconductors,” *Nature*, vol. 612, pp. 647–657, Dec. 2022.
- [28] J.-X. Yin, W. Ma, T. A. Cochran, X. Xu, S. S. Zhang, H.-J. Tien, N. Shumiya, G. Cheng, K. Jiang, B. Lian, Z. Song, G. Chang, I. Belopolski, D. Multer, M. Litskevich, Z.-J. Cheng, X. P. Yang, B. Swidler, H. Zhou, H. Lin, T. Neupert, Z. Wang, N. Yao, T.-R. Chang, S. Jia, and M. Zahid Hasan, “Quantum-limit Chern topological magnetism in TbMn₆Sn₆,” *Nature*, vol. 583, pp. 533–536, July 2020.
- [29] J.-X. Yin, S. S. Zhang, H. Li, K. Jiang, G. Chang, B. Zhang, B. Lian, C. Xiang, I. Belopolski, H. Zheng, T. A. Cochran, S.-Y. Xu, G. Bian, K. Liu, T.-R. Chang, H. Lin, Z.-Y. Lu, Z. Wang, S. Jia, W. Wang, and M. Z. Hasan, “Giant and anisotropic many-body spin-orbit tunability in a strongly correlated kagome magnet,” *Nature*, vol. 562, pp. 91–95, Oct. 2018.
- [30] M. Kang, S. Fang, L. Ye, H. C. Po, J. Denlinger, C. Jozwiak, A. Bostwick, E. Rotenberg, E. Kaxiras, J. G. Checkelsky, and R. Comin, “Topological flat bands in frustrated kagome lattice CoSn,” *Nature Communications*, vol. 11, p. 4004, Aug. 2020.
- [31] C. Guo, G. Wagner, C. Putzke, D. Chen, K. Wang, L. Zhang, M. Gutierrez-Amigo, I. Errea, M. G. Vergniory, C. Felser, M. H. Fischer, T. Neupert, and P. J. W. Moll, “Correlated order at the tipping point in the kagome metal CsV₃Sb₅,” *Nature Physics*, vol. 20, pp. 579–584, Apr. 2024.
- [32] T. A. Empante, Y. Zhou, V. Klee, A. E. Nguyen, I.-H. Lu, M. D. Valentin, S. A. Naghibi Alwillar, E. Preciado, A. J. Berges, C. S. Merida, *et al.*, “Chemical vapor deposition growth of few-layer MoTe₂ in the 2H, 1T’, and 1T phases: tunable properties of MoTe₂ films,” *ACS nano*, vol. 11, no. 1, pp. 900–905, 2017.
- [33] J. Hafner, “Ab-initio simulations of materials using vasp: Density-functional theory and beyond,” *Journal of computational chemistry*, vol. 29, no. 13, pp. 2044–2078, 2008.
- [34] K. F. Garrity, J. W. Bennett, K. M. Rabe, and D. Vanderbilt, “Pseudopotentials for high-throughput dft calculations,” *Computational Materials Science*, vol. 81, pp. 446–452, 2014.
- [35] M. Lv, G. Yu, and W. Chen, “2D NbIrTe₄ and TaRhTe₄ monolayers: Two fascinating topological insulators as electrocatalysts for oxygen reduction,” *Inorg. Chem. Front.*, vol. 9, no. 23, pp. 6133–6146, 2022.
- [36] A. A. Mostofi, J. R. Yates, Y.-S. Lee, I. Souza, D. Vanderbilt, and N. Marzari, “wannier90: A tool for obtaining maximally-localised wannier functions,” *Computer physics communications*, vol. 178, no. 9, pp. 685–699, 2008.
- [37] G. W. Bryant, “Surface states of ternary semiconductor alloys: effect of alloy fluctuations in one-dimensional models with realistic atoms,” *Physical Review B*, vol. 31, no. 8, p. 5166, 1985.
- [38] A. A. Soluyanov and D. Vanderbilt, “Wannier representation of Z_2 topological insulators,” *Physical Review B*, vol. 83, no. 3, p. 035108, 2011.
- [39] H. Fröhlich, “On the theory of superconductivity: the one-dimensional case,” *Proceedings of the Royal Society of London. Series A. Mathematical and Physical Sciences*, vol. 223, no. 1154, pp. 296–305, 1954.